On the runup of long waves on a plane beach

I-Chi Chan[1] and Philip L.-F. Liu[1,2]

Received 18 February 2012; revised 4 June 2012; accepted 11 June 2012; published 3 August 2012.

[1] Using the records of free surface fluctuations at several locations during the 2011 Japan Tohoku tsunami, we first show that the leading tsunami waves in both near-field and far-field regions are small amplitude long waves. These leading waves are very different from solitary waves. We then focus on investigating the evolution and runup of non-breaking long waves on a plane beach, which is connected to a constant depth region. For this purpose, we develop a Lagrangian numerical model to solve the nonlinear shallow water equations. The Lagrangian approach tracks the moving shoreline directly without invoking any additional approximation. We also adopt and extend the analytical solutions by Synolakis (1987) and Madsen and Schäffer (2010) for runup and rundown of cnoidal waves and a train of multiple solitary waves. The analytical solutions for cnoidal waves compare well with the existing experimental data and the direct numerical results when wave amplitudes are small. However, large discrepancies appear when the incident amplitudes are finite. We also examine the relationship between the maximum runup height and the leading wave form. It is concluded that for a single wave the accelerating phase of the incident wave controls the maximum runup height. Finally, using the analytical solutions for the approximated wave forms of the leading tsunamis recorded at Iwate South station from the 2011 Tohoku Japan tsunami, we estimate the runup height.

Citation: Chan, I-C., and P. L.-F. Liu (2012), On the runup of long waves on a plane beach, *J. Geophys. Res.*, *117*, C08006, doi:10.1029/2012JC007994.

1. Introduction

[2] Analytical solutions for non-breaking long waves running up a plane beach have been well studied. *Carrier and Greenspan* [1958] obtained the exact solution for the nonlinear shallow water equations by assuming that the plane beach extends to infinity. *Keller and Keller* [1964] derived the analytical solution for linear shallow water waves propagating on a constant water depth and then climbing up a plane beach (this "two-slope beach" is commonly called the canonical problem [see, e.g., *Synolakis et al.*, 2008]). Although the canonical problem is a more realistic bathymetry than that of *Carrier and Greenspan* [1958], *Keller and Keller*'s [1964] analytical solution can not describe the moving shoreline because of the adaptation of linear wave theory resulting in a fixed shoreline position. *Synolakis* [1987] linked together the two pioneering works by matching the nonlinear solution of *Carrier and Greenspan* [1958] with the linear solution of *Keller and Keller* [1964] at the toe of the plane beach. The full solution is given in terms of Fourier integrals involving Bessel functions. A closed form solution for the runup of solitary waves was further developed by adopting the asymptotic expressions for Bessel functions, under the condition that the amplitude-to-depth ratio of the incident solitary wave is much greater than the inverse of beach slope. We remark that *Gjevik and Pedersen* [1981] have also studied analytically the runup of solitary waves. However, their solution is less accurate than that of *Synolakis* [1987] as they approximated the solitary wave profile with the elevated half of a sine wave. The work of *Synolakis* [1987] is quite significant in the sense that solitary waves have been widely used as model waves for tsunami research in both laboratory experiments and numerical simulations since the 1970s. More specifically, *Synolakis* [1987] deduced an analytical runup formula allowing a simple estimation on the maximum runup heights of non-breaking solitary waves. This analytical solution, which has been shown to agree well with numerous laboratory measurements, has become a benchmark exercise for testing numerical models [*Synolakis et al.*, 2008].

[3] *Madsen et al.* [2008] recently demonstrated that real-world large scale tsunamis would not evolve into solitary waves in the geophysical scale. Consequently, *Madsen and Schäffer* [2010] extended *Synolakis*'s [1987] work and developed closed form solutions for the runup of linear periodic progressive waves and a transient wave form whose surface elevation is described by $\mathrm{sech}^2(\cdot)$-profile (i.e., it is similar to a solitary wave form, but the effective wavelength is independent of wave height). Analytical solutions for

[1]School of Civil and Environmental Engineering, Cornell University, Ithaca, New York, USA.
[2]Institute of Hydrological and Oceanic Sciences, National Central University, Jhongli, Taiwan.

Corresponding author: I-C. Chan, School of Civil and Environmental Engineering, Cornell University, 220 Hollister Hall, Ithaca, NY 14853, USA. (ic63@cornell.edu)

0148-0227/12/2012JC007994

general incident wave forms are also obtained in terms of convolution integrals involving the first and second time derivatives of surface elevation record of the incident wave. We note that *Madsen and Schäffer* [2010] also used the asymptotic approximations of Bessel functions in deducing their solutions.

[4] The objectives of this paper are multiple: (1) To provide further evidence to support *Madsen et al.*'s [2008] claim that the leading waves of a real-world tsunami can not be modeled by solitary waves. (2) To assess the performance of the analytical solutions developed by *Madsen and Schäffer* [2010] for various incident wave scenarios. (3) To provide new analytical and numerical results of runup for more complex incident waves. We organize this note in the following manner. In section 2.1 we analyze some of the field data of free surface elevations taken during the 2011 Japan Tohoku tsunami to show that the leading tsunami waves in both near-field (close to the epicenter) and far-field can not be characterized as solitary waves. We further demonstrate that the leading tsunami waves at Iwate South station can be adequately modeled by a linear superposition of three $\mathrm{sech}^2(\cdot)$ wave forms. In the deep ocean basin, both wave nonlinearity and frequency dispersion of the leading waves are small and insignificant. In section 2.2 the analytical solutions of wave runup by *Madsen and Schäffer* [2010] are reviewed and extended to consider the incident wave as a series of periodic waves or $\mathrm{sech}^2(\cdot)$ waves. In sections 2.3 and 2.4 the formulation of Lagrangian numerical model is described, and the comparisons between the analytical solutions and numerical results are presented, respectively. The advantage of the Lagrangian description is that the shoreline movement is tracked exactly. The comparisons show that the analytical solutions are reasonably accurate as long as the incident waves are indeed linear waves. The advantage of the analytical solutions is that it can be computed very quickly. In section 3.1 we extend the analytical solutions for the runup of cnoidal waves. New formulae for describing the shoreline movements are derived. Analytical solutions are compared with the existing experimental data and the direct (Lagrangian) numerical results. In section 3.2 we discuss the runup and rundown processes of two successive solitary waves, which can have different wave heights. The runup height of the second wave can be larger or smaller than that of the first wave depending on the wave height ratio and the time lapse between two wave crests. In section 3.3 we apply the general runup formula to estimate the maximum runup height using the wave record at Iwate South as the incident wave. In section 4 we return to the discussion of the key factors affecting the maximum runup height. Examples are given to show that the maximum runup height is determined by the acceleration of the leading wave.

2. Characteristics of Leading Tsunami Waves and Theoretical Models

[5] Tsunamis are extremely long waves often triggered by submarine earthquakes. Solitary waves have long been employed for modeling many important features of tsunamis, including runup processes on a coast [*Synolakis*, 1987]. The solitary wave paradigm for tsunamis research arose from a series of theoretical and experimental studies by Hammack and Segur [see, e.g., *Hammack and Segur*, 1978] in the 1970s, who pointed out that the leading wave of an initial free surface hump with a net positive volume will eventually evolve into a solitary wave after traveling a long distance. Since solitary wave remains its permanent form both spatially and temporally, it is convenient to employ solitary wave as a model for the leading tsunami wave in performing laboratory experiments and in deriving theoretical results. However, *Madsen et al.* [2008] cautioned that the leading wave of a real-world tsunami is not a solitary wave because the required evolutionary distance far exceeds the width of any ocean on the Earth. In fact, this issue was addressed implicitly in the original works by Hammack and Segur (see the review by *Segur* [2007]). In this section we shall re-iterate the difference between solitary waves and leading waves of real-world tsunamis by reviewing briefly the solitary wave theory and comparing the solitary wave solution with the field observations from the 2011 Japan Tohoku tsunami.

2.1. Characteristics of Solitary Waves and Leading Tsunami Waves

[6] On a constant water depth, h_0, the surface profile of a solitary wave can be expressed as

$$\zeta(x,t) = H\mathrm{sech}^2[k(x - x_0 - ct)], \tag{1}$$

where H is the wave height, x_0 is the location of the wave crest at $t = 0$, $c = \sqrt{g(h+H)}$ denotes the wave speed with g being the gravitational acceleration, and the *effective* wave number k is defined as

$$k = k_0 = \frac{1}{h_0}\sqrt{\frac{3}{4}\frac{H}{h_0}}. \tag{2}$$

The effective wavelength, L, and wave period, T, can be defined as $L = 2\pi/k$ and $T = 2\pi/kc$, respectively. Equation (1), with $k = k_0$, satisfies the Korteweg-de Vries equation, which requires specifically the balance of weak nonlinearity ($\epsilon = H/h_0 \ll 1$) and moderate frequency dispersion ($\mu = h_0/L \ll 1$), i.e., $O(\epsilon) \sim O(\mu^2)$. The theory is restrictive in the sense that the effective wavelength and the effective wave period of a solitary wave are constrained by the wave height for a specified water depth. Therefore, the higher the wave height is, the shorter the effective wavelength becomes.

[7] We now examine some of the water surface elevation data of the 2011 Japan Tohoku tsunami with respect to the solitary wave theory. Figure 1 shows the time histories of leading tsunami waves at three stations near the epicenter. As indicated in Figure 1a, the ocean bottom pressure gage stations (TM1 and TM2) and the GPS-based station (Iwate South) are roughly located along a straight-line. Using the ETOPO1 database, the bathymetry along the transect is shown in Figure 1b. The linear slope between TM1 and Iwate South is roughly 1 : 42. In Figure 1c the time histories of surface elevation at these three stations are plotted. The coordinates and the water depths at these stations, and several other physical parameters obtained using the information presented in Figure 1 are listed in Table 1. We note that based on the surface elevation measurements the wave nonlinearity, $\epsilon = H/h$, is extremely small in all three stations; the largest wave appeared at Iwate South with $\epsilon = 0.033$. From the measurements we further estimate the wave period

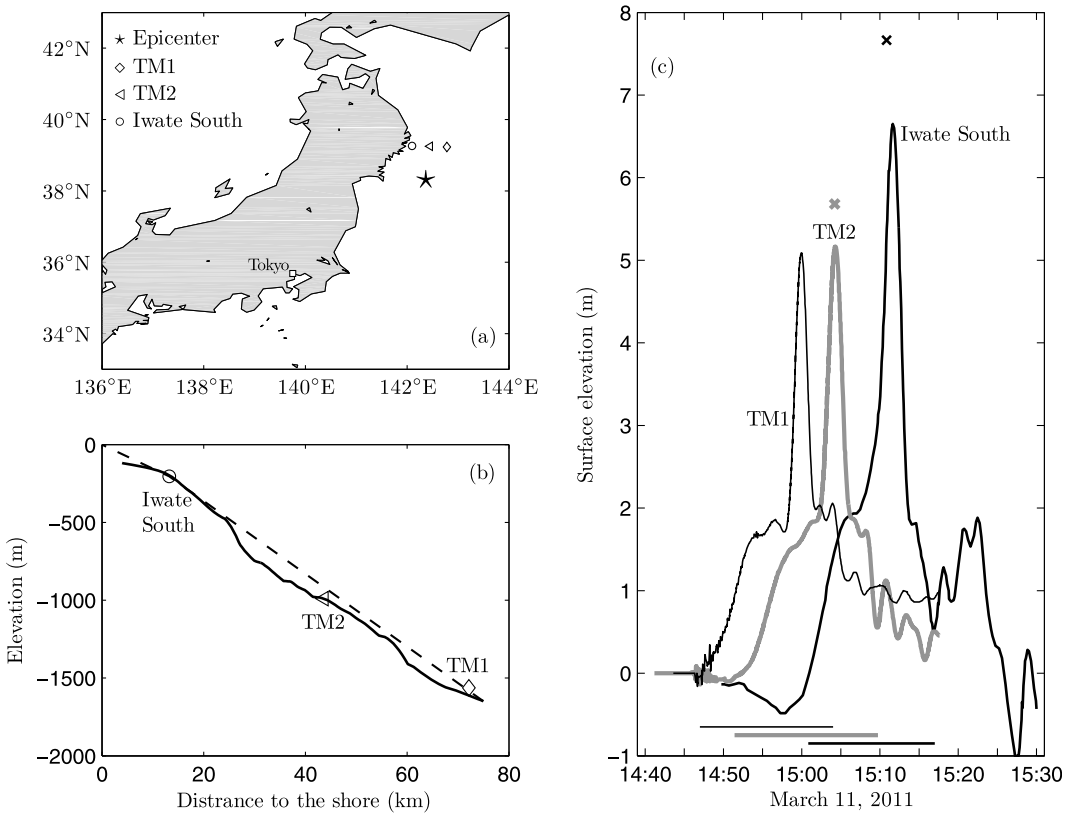

Figure 1. Observations of 2011 Tohoku tsunami near the epicenter. (a) Locations of the epicenter, ocean bottom pressure gauges (TM1 and TM2), and the GPS-based wave station (Iwate South). (b) Approximate bathymetry by assuming that three stations are in a line. Solid line is derived from the ETOPO1 database; dashed line depicts a 1 : 42 linear slope. (c) Records of free surface elevation at these three stations during the main event. The crosses denote the arrival time and the amplitude of the main peak estimated by the linear phase speed and Green's law. Horizontal lines depict our estimation of the wave periods. Measurements are digitized from *Fujii et al.* [2011].

as $T = 17$ minutes (Figure 1c). The effective wavelength at each station can then be estimated by using $L = T\sqrt{gh}$, as listed in Table 1. Clearly, as the wave propagated into shallower water the wavelength decreased. The corresponding values of frequency dispersiveness parameter, $\mu = h/L$, are also very small, suggesting that the frequency dispersion effect is negligible. In fact, since $O(1) \gg O(\epsilon) \gg O(\mu^2)$, the linear shallow water wave theory can adequately describe the wave propagation process from TM1 to Iwate South. Using the linear long-wave celerity based on the averaged depth between two adjacent stations and the Green's Law, we calculated the arrival time of the peak of the leading waves and the corresponding wave height at TM2 and Iwate South, respectively, as denoted by crosses in Figure 1c. Indeed, the linear shallow wave theory gives accurate estimations on the arrival time, although the wave amplitude is overestimated. Noted that the discrepancy could be caused by horizontal wave energy spreading and energy dissipative effects that were not included in our rough estimation. In Figure 2, we compare a solitary wave form with the field data at Iwate South. Using the nonlinearity, $\epsilon = H/h = 0.033$, the effective wavelength of the solitary wave can be calculated from (2), resulting in an effective wave period of $T = 3$ minutes that is much shorter than that of the observed data. In the same figure we further impose a $\mathrm{sech}^2(\cdot)$-profile with a period of $T = 12$ minutes (i.e., $k = 0.25k_0$ in (1) and (2)). Visually, this wave form captures the surface profile in the vicinity of the main peak quite reasonably, but it does not describe the leading depression wave and the following secondary elevated wave. The free surface profile of the leading waves at Iwate South can be better fitted by a combination of three $\mathrm{sech}^2(\cdot)$ profiles (see Figure 2):

$$\zeta(t) = \sum_{n=1}^{3} H_n \mathrm{sech}^2 \Omega_n (t - (t_0 + t_n)), \tag{3}$$

Table 1. Physical Parameters for Leading Waves of 2011 Tohoku Tsunami Recorded at Three Select Stations Shown in Figure 1[a]

Station	x	h	H	L	$(H/h) \times 10^3$	$(h/L)^2 \times 10^4$
TM1	72	1618	5.1	130	3.20	1.55
TM2	44	1013	5.2	100	5.10	1.03
Iwate South	14	204	6.7	45	32.80	2.06

[a]Here, x (km): estimated distance from the shore; h (m): water depth; H (m): maximum surface elevation; L (km): estimated effective wavelength.

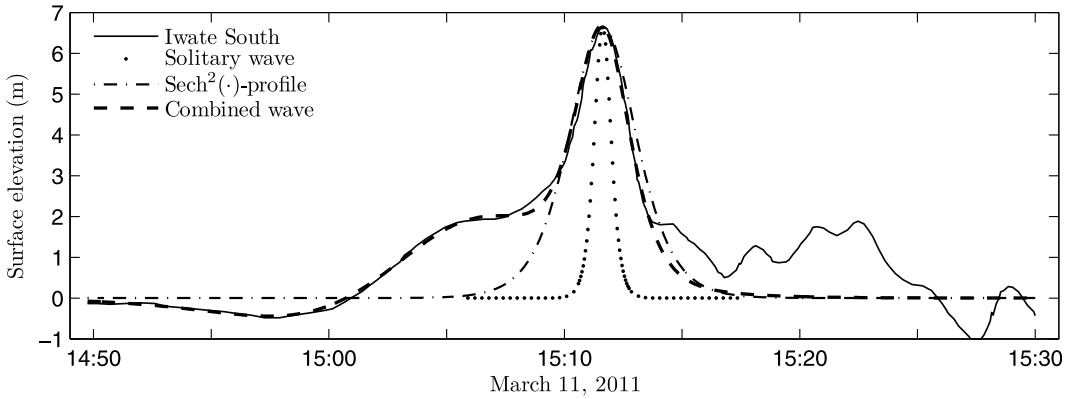

Figure 2. Records of surface elevation at the Iwate South GPS station. Solid: field observation. Dot: solitary wave solution, i.e., (1) with $k = k_0$ defined in (2). Dashed-dotted: sech$^2(\cdot)$ profile with $k = 0.25k_0$. Dashed: a combination of three sech$^2(\cdot)$ profiles given by (3).

where the coefficients are

$$\begin{cases} (H_1, \Omega_1, t_1) = (-0.80, 0.179, 19.67) \\ (H_2, \Omega_2, t_2) = (2.20, 0.198, 26.33) \\ (H_3, \Omega_3, t_3) = (5.85, 0.653, 31.63) \end{cases}$$

with the units (m, min^{-1}, min), respectively, and the reference t_0 being 14:50 on March 11. In section 3.3 we will discuss the estimation of the maximum runup height caused by these approximated incident waves on a plane beach.

[8] As the distance between stations TM1 and Iwate South is less than 80 km (see Figure 1), which is shorter than the estimated wavelengths at TM1 and TM2, it is not so surprising that the leading tsunami wave is not a solitary wave. To seek for further evidence we examine the eastbound tsunami waves propagating across the fetch of the Pacific Ocean. Based on the tsunami data posted by NOAA PMEL (http://nctr.pmel.noaa.gov/honshu20110311/), free surface records from four DART buoys are selected for analyses and further discussions. These stations are roughly located along one of main wave propagation directions; their locations and the records of surface fluctuations are plotted in Figure 3. The associated wave parameters are also listed in Table 2. DART 21413 is relatively close to the epicenter (about 1244 km to the east). The leading wave at this station has an estimated effective wave period of 38 minutes with a wave amplitude (crest) of 80 cm and a wave trough of 33 cm. At the far field DART stations (more than 10000 km away from the epicenter), the evolution of leading waves from DART 51406 to DART 32401 (see Figures 3b–3d) can be clearly seen. The first elevated wave appears to separate from the main wave packet due to the frequency dispersion. However, these leading waves are not solitary waves; since their wave period is around 20 min, while the corresponding solitary wave with comparable wave height has a much longer period of 13.6 hr (using $\epsilon = 10^{-5}$ with $h = 4500$ m). In other words, the first elevated wave has a wavelength roughly 300 km, while the solitary wave is at least 30 times wider. We also observe that the linear theory indeed predicts reasonably well the propagation speed of leading waves, as can be seen from the arriving time listed in Table 2 and the wave records shown in Figure 3.

[9] Through examining the westbound and the eastbound leading tsunamis of the 2011 event, we have demonstrated that solitary waves are not proper model waves for leading tsunami waves. We also observe that on the continental shelf leading tsunami waves are much longer than the solitary waves with comparable wave height, while in deep ocean the opposite is true. This behavior has also been reported for the 2004 Indian Ocean tsunami as the leading waves propagating across the Bay of Bengal (see the numerical simulations by *Wang and Liu* [2007]).

2.2. Theoretical Model in the Eulerian Description

[10] Based on the field evidence presented in the previous section, we observe that the effect of frequency dispersion on leading tsunami waves is insignificant when the leading waves propagate over only short distances relative to the wavelengths (e.g., Figures 1, 3c, and 3d). Nevertheless, the accumulated dispersion effect can be considerable after the leading wave has propagated over a long distance, which is demonstrated by the comparison between Figures 3b and 3d. As for the nonlinear effect, it is shown to be even less important when tsunamis propagate in the ocean basin and continental shelf. However, nonlinearity becomes increasingly significant as the leading waves run up a coast, while the frequency dispersion effects decrease. In practice, nonlinear shallow water equations are often used to describe the propagation and runup of leading tsunamis in the coastal region [see, e.g., *Wang and Liu*, 2007]. In terms of the depth-averaged velocity, u, and free-surface displacement, ζ, the two-dimensional (i.e., one horizontal dimension) nonlinear shallow water equations are:

$$\frac{\partial \zeta}{\partial t} + \frac{\partial}{\partial x}[u(h+\zeta)] = 0 \tag{4}$$

and

$$\frac{\partial u}{\partial t} + u\frac{\partial u}{\partial x} = -g\frac{\partial \zeta}{\partial x}, \tag{5}$$

where $h = h(x)$ is the varying depth. These equations can be solved numerically in general. Analytical solutions have also been obtained if the bathymetry is an uniformly sloping

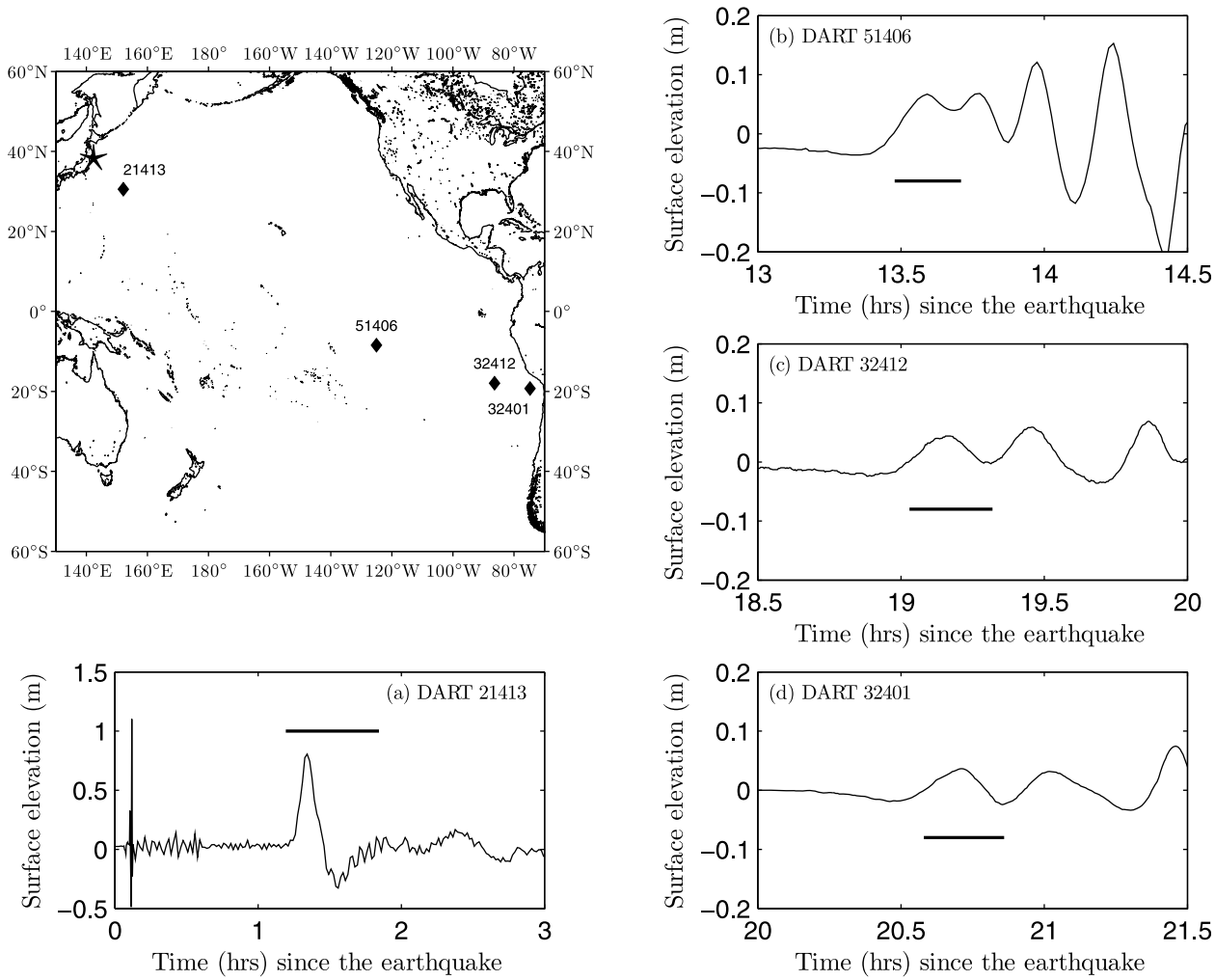

Figure 3. 2011 Tohoku tsunami: records of surface fluctuations at four select DART buoys. The epicenter is marked by the star. Horizontal bars denote our estimations of wave periods for the leading elevated waves.

beach or a two-slope beach (i.e., the canonical problem: a constant slope being connected to a constant depth region).

[11] For a canonical problem, *Synolakis* [1987] and *Madsen and Schäffer* [2010] obtained analytical solutions for the velocity u and free surface elevation ζ at the moving shoreline as (U, R):

$$U(\tau) = \frac{1}{s}\sqrt{\frac{2}{\pi}}\int_{-\infty}^{\infty} \frac{\mathrm{i}\omega \exp(-\mathrm{i}\omega\tau)\mathcal{F}\{\Phi(t)\}}{J_0(2\omega t_0) - \mathrm{i}J_1(2\omega t_0)}\, d\omega,$$
$$R(\tau) = \sqrt{\frac{2}{\pi}}\int_{-\infty}^{\infty} \frac{\exp(-\mathrm{i}\omega\tau)\mathcal{F}\{\Phi(t)\}}{J_0(2\omega t_0) - \mathrm{i}J_1(2\omega t_0)}\, d\omega - \frac{U^2}{2g}, \tag{6}$$

where s is the beach slope, $\tau = t - U(\tau)/sg$ translates between the transformed time variable, τ, and the physical time, t, $J_n(\cdot)$ is the Bessel function of the first kind,

$$t_0 = \frac{X_0}{\sqrt{gh_0}} = \frac{h_0/s}{\sqrt{gh_0}} \tag{7}$$

with X_0 and h_0 representing the location of the toe of the slope and the constant water depth, respectively, $\mathcal{F}\{\cdot\}$ denotes the Fourier transform with respect to time, and

$$\Phi(t) = \zeta_{\mathrm{inc}}(X_0, t) \tag{8}$$

is the incident wave record at the beach toe. Approximating the Bessel functions by their asymptotic expressions for

Table 2. Physical Parameters Associated With the Wave Data Recorded at Four DART Buoys (See Figure 3)[a]

Station	x	h	H	t_c	$(H/h) \times 10^5$	$(h/L)^2 \times 10^4$
DART 21413	1244	5874	80.6	1.34	13.70	1.09
DART 51406	10817	4450	6.7	13.59	1.50	6.50
DART 32412	14800	4364	4.4	19.15	1.00	4.08
DART 32401	15867	4800	3.6	20.72	0.75	4.82

[a]Here, x (km): distance from the epicenter; h (m): water depth; H (cm): amplitude of the first elevated wave; t_c (hr): arriving time (after the earthquake) of the first wave crest. $L = T\sqrt{gh}$ is the estimated wavelength with wave periods, T, defined in Figure 3. DART 21413 is about 1275 km southeast of Tokyo, Japan and DART 32401 is about 480 km away from Arcia, Chile.

large arguments, *Madsen and Schäffer* [2010] simplified the above solutions as

$$U(\tau) = -\frac{2\sqrt{t_0}}{s}\int_{2t_0}^{\tau}\frac{F_u(\tau - t)}{\sqrt{\tau - 2t_0}}dt,$$
$$R(\tau) = 2\sqrt{t_0}\int_{2t_0}^{\tau}\frac{F_\zeta(\tau - t)}{\sqrt{\tau - 2t_0}}dt - \frac{U^2}{2g}, \tag{9}$$

where $F_u(t) = \frac{\partial}{\partial t}F_\zeta(t) = \frac{\partial^2}{\partial t^2}\Phi(t)$. This approximation is reasonable when $t_0 > 0.4T$, where T is the wave period of the incident wave [*Madsen and Schäffer*, 2010]. In fact, the asymptote condition has also been discussed analytically by *Synolakis* [1987] and numerically by *Liu and Cho* [1994].

[12] For special cases in which the incident wave record, $\Phi(t)$, is a linear progressive wave or can be described by a single $\mathrm{sech}^2(\cdot)$-profile (i.e., in the form of (1) but with an arbitrary k), *Madsen and Schäffer* [2010] further deduced the closed form solutions for $U(\tau)$ and $R(\tau)$. Using their fundamental solutions, it is straightforward to show that for an incident wave that can be cast as

$$\Phi(t) = \sum_{n=1}^{N} A_n \cos\,\Omega_n(t - t_n) \tag{10}$$

with A_n, Ω_n, and t_n being the wave amplitude, wave frequency, and arbitrary phase shift, respectively, the corresponding runup solutions (U, R) are:

$$U(\tau) = \sum_{n=1}^{N}\frac{\Omega_n}{s}R_n^0\sin\left(\theta_n + \frac{\pi}{4}\right),$$
$$R(\tau) = \sum_{n=1}^{N}R_n^0\cos\left(\theta_n + \frac{\pi}{4}\right) - \frac{U^2}{2g}, \tag{11}$$

where $R_n^0 = 2A_n\sqrt{\pi\Omega_n t_0}$ and $\theta_n = \Omega_n(\tau - t_n - 2t_0)$. On the other hand, if the incident wave can be expressed as

$$\Phi(t) = \sum_{n=1}^{N} H_n \mathrm{sech}^2[\Omega_n(t - t_n)], \tag{12}$$

we obtain the following solutions:

$$U(\tau) = \sum_{n=1}^{N} 2\frac{\Omega_n}{s}R_n^0\mathrm{Li}\left(-\frac{5}{2}, -e^{2\theta_n}\right),$$
$$R(\tau) = \sum_{n=1}^{N} - R_n^0\mathrm{Li}\left(-\frac{3}{2}, -e^{2\theta_n}\right) - \frac{U^2}{2g}, \tag{13}$$

where $R_n^0 = 8H_n\sqrt{2\pi\Omega_n t_0}$, $\theta_n = \Omega_n(\tau - t_n - 2t_0)$, and $\mathrm{Li}(m, z)$ denotes the polylogarithm (Jonquièrès function). In addition to the runup solutions U and R, the corresponding theoretical breaking condition, i.e., $\zeta_x \to \infty$, is

$$\frac{1}{sg}\frac{\partial U(\tau)}{\partial \tau} = -1. \tag{14}$$

[13] The above analytical solutions can be computed quickly for illustrating the time history of the shoreline location. In the later sections, we will demonstrate that these solutions can be applied to investigate the runup of more complicated incoming waves. In closing, we remark here that in obtaining the analytical solution in the integral form, (9), the incident waves must be linear at the toe of the slope. In general, this is a reasonable approximation for leading tsunami waves.

2.3. Lagrangian Nonlinear Long-Wave Model

[14] To complement the above analytical solutions, we develop a numerical model based on the Lagrangian nonlinear shallow water theory [*Goto*, 1979]:

$$\left(1 + \frac{\partial X}{\partial a}\right)\frac{\partial^2 X}{\partial t^2} = -g\frac{\partial}{\partial a}\left[\frac{h(a)}{1 + \frac{\partial X}{\partial a}} - h(a + X)\right], \tag{15}$$

where $X = X(a, t)$ is the horizontal displacements of particles initially occupying the undisturbed free surface. The relationship between the Lagrangian coordinate, a, and the horizontal Cartesian coordinate, x, is $x = a + X(a, t)$. The corresponding theoretical limitation (or wave breaking) requires $\partial X/\partial a \geq -1$. Using the Lagrangian approach, we can accurately and directly calculate the time history of the shoreline movement, including the position and the velocity (see the review by *Fujima* [2007]).

[15] The model equation, (15), is solved numerically by an explicit finite difference scheme on uniform grids. The time derivative is approximated by three-point explicit scheme and the spatial derivatives are evaluated using five-point formulas. The current numerical model can be used to study the runup of general incident wave forms over an arbitrary topography. The incident wave does not have to be linear as required by the analytical solutions. These are the advantages of numerical modeling over the existing analytical approaches. We have tested our numerical solutions against two benchmark problems. The first case is the runup of a periodic wave on a uniformly sloping beach (can be viewed as a boundary-value problem [see *Carrier and Greenspan*, 1958]). The second case is the evolution and runup of an initially static disturbance (initial-value problem [see *Carrier et al.*, 2003; *Kânoğlu*, 2004]). In both cases nearly perfect agreement is observed. We have also tested the performance of our numerical model for simulating a solitary wave propagating over a constant depth h_0. In the case where $\epsilon = 0.01$ the numerical results show that the solitary wave remains the same shape within a traveling distance of $100h_0$.

2.4. Comparisons Between Eulerian Solutions and Lagrangian Results

[16] We shall use our numerical model to discuss the performance of the analytical solutions obtained by *Madsen and Schäffer* [2010]. Figure 4 shows the runup of a solitary wave on a two-slope beach. The initial wave nonlinearity is $\epsilon = 0.01$ and the beach slope is $s = 1/20$. Numerical results are compared with the approximate shoreline solutions given in (13) (with $N = 1$) as well as the integral solutions obtained by *Synolakis* [1987] (i.e., equation (6)). In this example, the convergence of our numerical results is first confirmed as shown in Figure 4. The numerical solutions match well with those of *Synolakis* [1987] at three selected locations: $x/X_0 = 1.0$, 0.5, 0.25, where X_0 is the position of the beach toe; see Figures 4b–4d. However, as shown in Figure 4a the difference around the maximum runup can be seen.

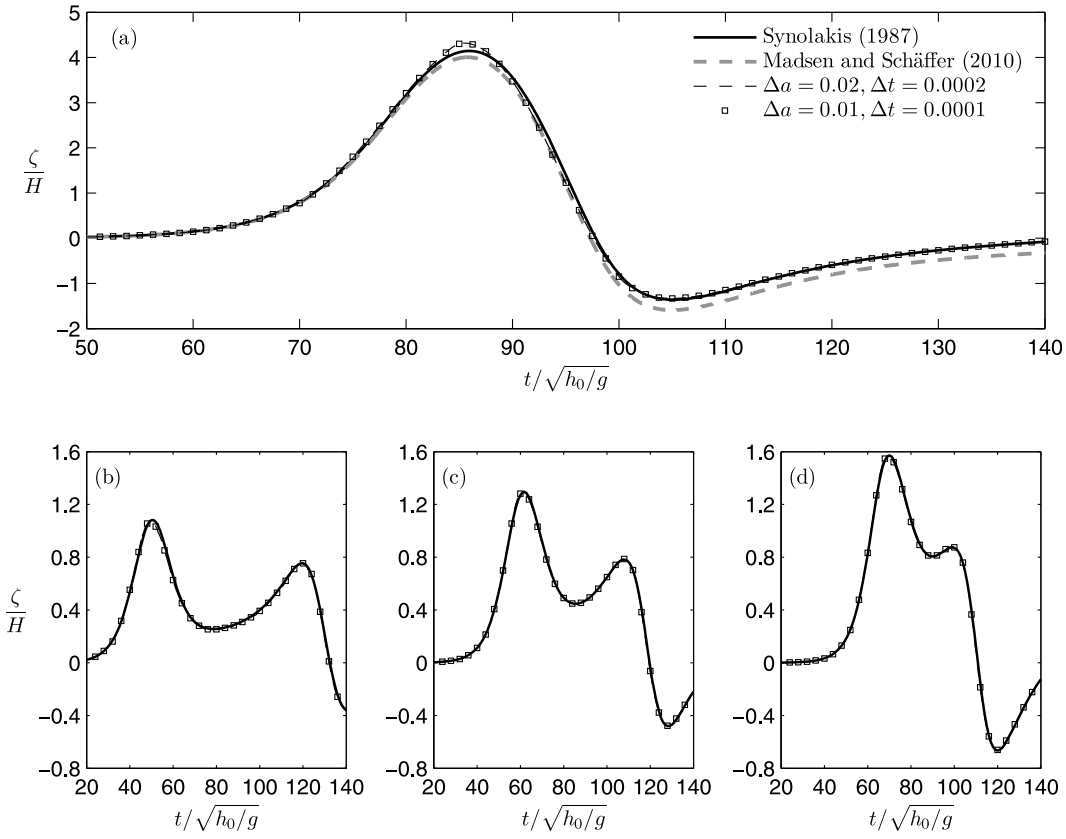

Figure 4. Runup of a solitary wave on a two-slope beach: $\epsilon = 0.01$, $s = 1/20$. (a) Time history of the shoreline position. (b) Time history of surface elevation at the beach toe, $x = X_0$. (c and d) Time histories of surface elevation at $x/X_0 = 0.5, 0.25$, respectively, on the sloping beach. Two sets of numerical calculations are compared with the integral solutions of *Synolakis* [1987] (similar to those given in (9)) and the approximate shoreline solution by *Madsen and Schäffer* [2010] (i.e., (13) with $N = 1$). Numerical resolutions, (Δa, Δt), are normalized by h_0 and $\sqrt{h_0/g}$, respectively.

Regarding the analytical runup solutions by *Madsen and Schäffer* [2010], the discrepancy is appreciable when compared with the other two solutions. Nevertheless, the overall agreement is good.

[17] To further test the limitation of analytical solutions, we consider a non-breaking solitary wave of $\epsilon = 0.12$ running up a steep slope of $s = 1/2.75$ (i.e., a 20° slope). Using the Lagrangian numerical model we first calculate the evolution of the solitary wave in a constant depth. For this finite amplitude solitary wave the wave steepening in the constant depth region is considerable, due to the lack of frequency dispersion in our nonlinear shallow water model (see Figure 5a). For a fair comparison, this wave record is used as the input for the analytical runup estimation. In Figures 5b and 5c, we compare the entire time history of the free surface elevation at the beach toe and the shoreline solutions, respectively. The discrepancy between the analytical solutions and the numerical results is quite significant, which is caused by the fact that the requirement for a linear incident wave in the analytical solutions has clearly been violated [see also *Li and Raichlen*, 2001].

[18] Despite the limitation demonstrated in the finite amplitude incident wave example, we still consider the analytical solution approach (i.e., the results given by (9)) as a valuable tool since it requires little computational effort but yields very reasonable estimations. In the remainder of the paper we shall continue to explore applications of these different solution approaches with respect to more complex incident waves.

3. Runup of a Train of Waves

[19] We have mentioned briefly that the analytical solutions of *Madsen and Schäffer* [2010] can be extended to estimate the shoreline evolution generated by complex incident wave forms if the incident waves can be cast as a series of sinusoidal waves or $\mathrm{sech}^2(\cdot)$ profiles. Here we apply this idea to study the runup of cnoidal waves and multiple solitary waves. Numerical solutions are also obtained for verification purpose. Finally, we demonstrate the runup estimation based on the Iwate South GPS data.

3.1. Runup of Cnoidal Waves

[20] In a constant water depth, h_0, the free-surface elevation of cnoidal waves propagating in the negative x-direction can be obtained as [*Mei et al.*, 2005]:

$$\zeta(x,t) = \zeta_2 + H\mathrm{cn}^2\left(\frac{2K}{\lambda}(x+ct)\middle| m\right), \tag{16}$$

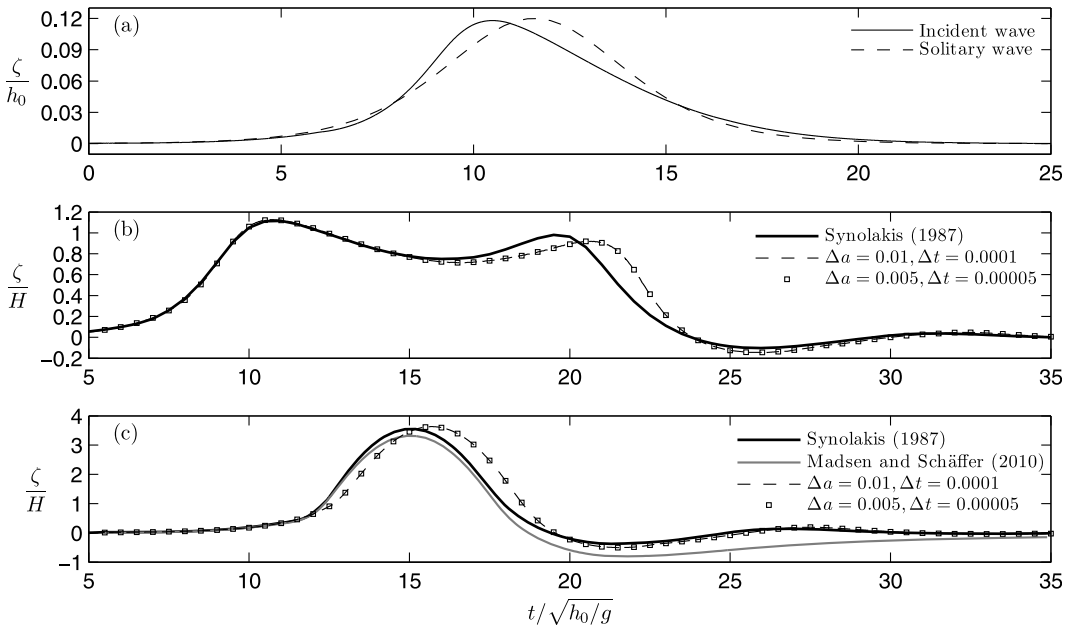

Figure 5. Solitary wave running up a two-slope beach: $\epsilon = 0.12$, $s = 1/2.75$. (a) Incident wave record at the beach toe, $x = 2.75h_0$. Dashed line plots a reference solitary wave solution with the initial wave crest located at $x = 15h_0$. (b) Records of surface elevation at the beach toe. (c) Time history of the shoreline position.

where *K(m)* and *E(m)* are, respectively, the complete elliptic integrals of the first and second kind, cn($z|m$) is the Jacobi elliptic function, and

$$\zeta_2 = \frac{H}{m}\left(1 - m - \frac{E(m)}{K(m)}\right),$$

$$\lambda = 2h_0 K(m)\sqrt{\frac{4}{3}\frac{h_0}{H}m},$$

$$c = \sqrt{gh_0}\left[1 + \frac{1}{m}\frac{H}{h_0}\left(1 - \frac{m}{2} - \frac{3}{2}\frac{E(m)}{K(m)}\right)\right].$$

In addition, the wave period can be defined as $T = \lambda/c$. The runup of cnoidal waves on a two-slope beach has been studied analytically by *Synolakis et al.* [1988]. Using the linear theory suggested by *Keller and Keller* [1964], they provided only the solution of maximum runup height, R_{up}:

$$\frac{R_{\mathrm{up}}}{h_0} = 2\zeta_2 + \frac{4\pi^2}{mK^2}\frac{H}{h_0} \max\left\{\sum_{i=0}^{\infty}\frac{q^{2i+1}}{\left(1+q^{2i+1}\right)^2} + \sum_{i=0}^{\infty}\sum_{j=0}^{\infty}\frac{q^{i+j+1}\left(\mathcal{M}_{ij}+\mathcal{N}_{ij}\right)}{\left(1+q^{2i+1}\right)\left(1+q^{2j+1}\right)}\right\}, \tag{17}$$

where $q = \exp(-\pi K'/K)$ with $K' = K(1 - m)$, and

$$\begin{cases} \mathcal{M}_{ij} = \sqrt{\widehat{k}_{ij}\pi X_0}\cos\left(\widehat{k}_{ij}(X_0 - ct) - \frac{\pi}{4}\right) \\ \mathcal{N}_{ij} = \sqrt{\widetilde{k}_{ij}\pi X_0}\cos\left(\widetilde{k}_{ij}(X_0 - ct) - \frac{\pi}{4}\right) \end{cases}$$

with $\widehat{k}_{ij} = 2\pi(i+j+1)/\lambda$ and $\widetilde{k}_{ij} = 2\pi|i-j|/\lambda$, respectively. We note that expression (17) is slightly different from the original solution given in *Synolakis et al.* [1988] to account for possible typos appeared in their solution (see (5) in their paper). The difference between two solutions will be illustrated later in Figure 9.

[21] In this section, we will derive the solutions for shoreline evolution by adopting the existing solutions of *Madsen and Schäffer* [2010]. It is known that (16) can be formally expressed in terms of a series of sinusoidal progressive waves as *Whittaker and Watson* [1927]:

$$\zeta(x,t) = \sum_{n=1}^{\infty}\widetilde{A}_n\cos\left(\widetilde{\Omega}_n\left(t - \widetilde{t}\right)\right), \tag{18}$$

where

$$\widetilde{A}_n = H\frac{2\pi^2}{mK^2}\frac{nq^n}{1-q^{2n}}, \quad \widetilde{\Omega}_n = \frac{2n\pi}{T}, \quad \widetilde{t} = -\frac{x}{c}.$$

Equation (18) represents an infinite spectrum of amplitude-decaying progressive waves, i.e., $A_n \to 0$, as $n \to \infty$. Following (11), we can readily obtain the runup solution for the cnoidal wave as:

$$\begin{aligned} U(\tau) &= \sum_{n=1}^{\infty}\frac{2\widetilde{A}_n}{s}\sqrt{\pi\widetilde{\Omega}_n^3 t_0}\sin\left(\widetilde{\theta}_n + \frac{\pi}{4}\right), \\ R(\tau) &= \sum_{n=1}^{\infty}2\widetilde{A}_n\sqrt{\pi\widetilde{\Omega}_n t_0}\cos\left(\widetilde{\theta}_n + \frac{\pi}{4}\right) - \frac{U^2}{2g}, \end{aligned} \tag{19}$$

where $\widetilde{\theta}_n = \widetilde{\Omega}_n(\tau - 2t_0 + X_0/c)$. From (14), we also obtain the breaking criterion as

$$\frac{H}{h_0}\sum_{n=1}^{\infty}\frac{4}{mK^2}\frac{nq^n}{1-q^{2n}}\left(\frac{\pi^2\widetilde{\Omega}_n^2 h_0}{s^2 g}\right)^{\frac{5}{4}}\sin\left(\widetilde{\theta}_n - \frac{\pi}{4}\right) = 1. \tag{20}$$

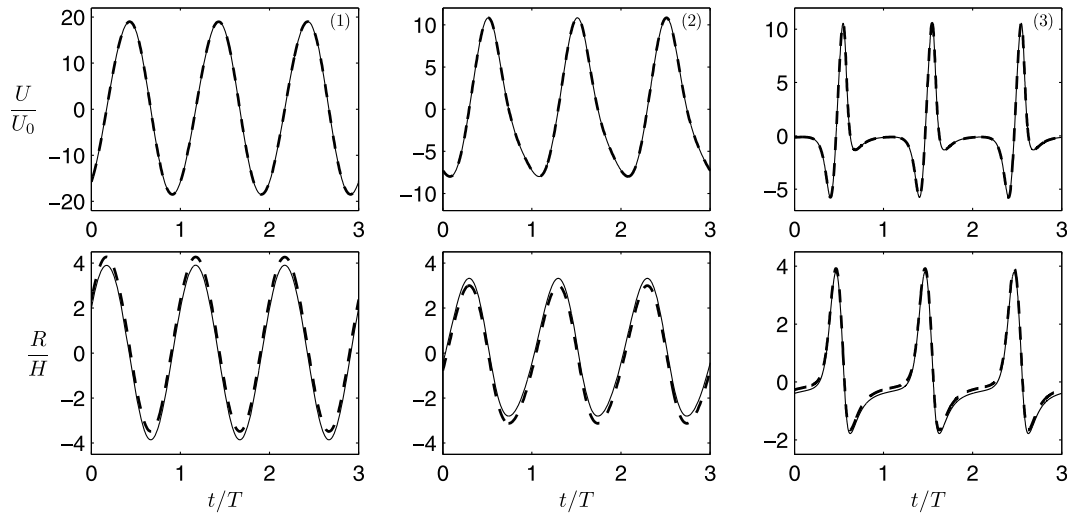

Figure 6. Cnoidal waves running up a two-slope beach with 1 : 20 slope. Case 1: $m = 0.05$, $\epsilon = 0.001$; case 2: $m = 0.5$, $\epsilon = 0.005$; case 3: $m = 0.9995$, $\epsilon = 0.01$. (top) The time histories of shoreline velocity, U. (bottom) The runup height, R. Solid lines show the analytical solutions by the sinusoidal approximation, i.e., (19). Dashed lines plot the solutions obtained from the soliton approximation, (22). $U_0 = c(H/h_0)$ is the reference velocity.

For a given slope s, the largest non-breaking cnoidal wave has a wave height H satisfying the above condition.

[22] We have obtained the runup solutions for cnoidal waves by treating the cnoidal waves as the superposition of a spectrum of sinusoidal waves. Alternatively, we can decompose the cnoidal wave solution, (16), into a series of soliton-like profiles [*Boyd*, 1984]:

$$\zeta(x,t) = \widehat{\zeta}_2 + \sum_{n=-\infty}^{\infty} \widehat{H}\,\mathrm{sech}^2\left[\widehat{\Omega}\left(t - \widehat{t}_n\right)\right], \tag{21}$$

where $\widehat{t}_n = nT - x/c$,

$$\widehat{\Omega} = \frac{\pi K}{TK'},\ \widehat{H} = \left(\frac{\pi}{2\sqrt{m}K'}\right)^2 H,\ \widehat{\zeta}_2 = \zeta_2 + \frac{H}{m}\left(m - \frac{E'}{K'}\right),$$

and $E' = E(1 - m)$. Following (13), we can express the runup solutions for the cnoidal waves as:

$$\begin{aligned} U(\tau) &= \sum_{n=-\infty}^{\infty} \frac{16}{s}\widehat{H}\sqrt{2\pi\widehat{\Omega}^3 t_0}\,\mathrm{Li}\left(-\frac{5}{2}, z_n\right), \\ R(\tau) &= \sum_{n=\infty}^{\infty} -8\widehat{H}\sqrt{2\pi\widehat{\Omega}t_0}\,\mathrm{Li}\left(-\frac{3}{2}, z_n\right) - \frac{U^2}{2g}, \end{aligned} \tag{22}$$

where $\widehat{\theta}_n = \widehat{\Omega}(\tau - 2t_0 - nT + X_0/c)$ and $z_n = -\exp\left(2\widehat{\theta}_n\right)$. We remark that, to be consistent with the approximation made in deriving (13), the contribution from the constant trough, $\widehat{\zeta}_2$, has been neglected in (22). More precisely, by formally requiring $2\omega t_0 \gg 1$ in (6), i.e., approximating the Bessel functions by their asymptotic forms at large arguments, any incident wave components with zero frequency will be omitted. This argument can be better understood from Figure 2 in *Madsen and Schäffer* [2010], which compares $(J_0(2\omega t_0) - \mathrm{i}J_1(2\omega t_1))^{-1}$ with its asymptotic approximation. We also note that the wave components with infinite periods have no effect in determining $U(\tau)$, as can be seen from (6).

[23] To demonstrate the above new solutions, we consider the following cnoidal waves: (1) $m = 0.05$, $\epsilon = H/h_0 = 0.001$; (2) $m = 0.5$, $\epsilon = 0.005$; (3) $m = 0.9995$, $\epsilon = 0.01$. The first case asymptotically represents a train of linear sinusoidal waves; the second example is a train of nonlinear periodic waves with higher and sharper wave crests and smaller and flatter troughs; finally the last case can be viewed as a train of soliton-like profiles connected by a negative trough. The wave nonlinearities are chosen such that all three wave trains will not break as they run up a 1 : 20 slope. In Figure 6, we first compare runup solutions obtained by using the sinusoidal approximation, i.e., (19), with those by the soliton approximation, (22). As can be seen, both solutions agree perfectly for *U(t)*. Regrading the time histories of runup height, *R(t)*, small discrepancies are observed for all three scenarios. This, in fact, is expected as employing different approximations for cnoidal waves would certainly result in different constant troughs.

[24] In Figure 7, we compare the runup of cnoidal waves with those of amplitude-comparable (i.e., same ϵ values) sinusoidal waves and solitary wave for cases 1 and 3, respectively. The runup solution of case 1 indeed resembles the behavior of a linear progressive wave. Because of the presence of a constant trough, the runup of cnoidal waves for case 3 is noticeably different from that of a solitary wave. For cases 2 and 3, i.e., $(m, \epsilon) = (0.5, 0.005)$ and $(m, \epsilon) = (0.9995, 0.01)$, respectively, we also compare the analytical solutions with the numerical results from our Lagrangian model. As shown in cases 2 and 3 in Figure 7, good agreements are observed for the both cases. We remark that in our numerical simulations a numerical wave-maker is installed at the far-end of the computational domain. The wave-maker moves with the prescribed motion for cnoidal waves as suggested by *Goring and Raichlen* [1980].

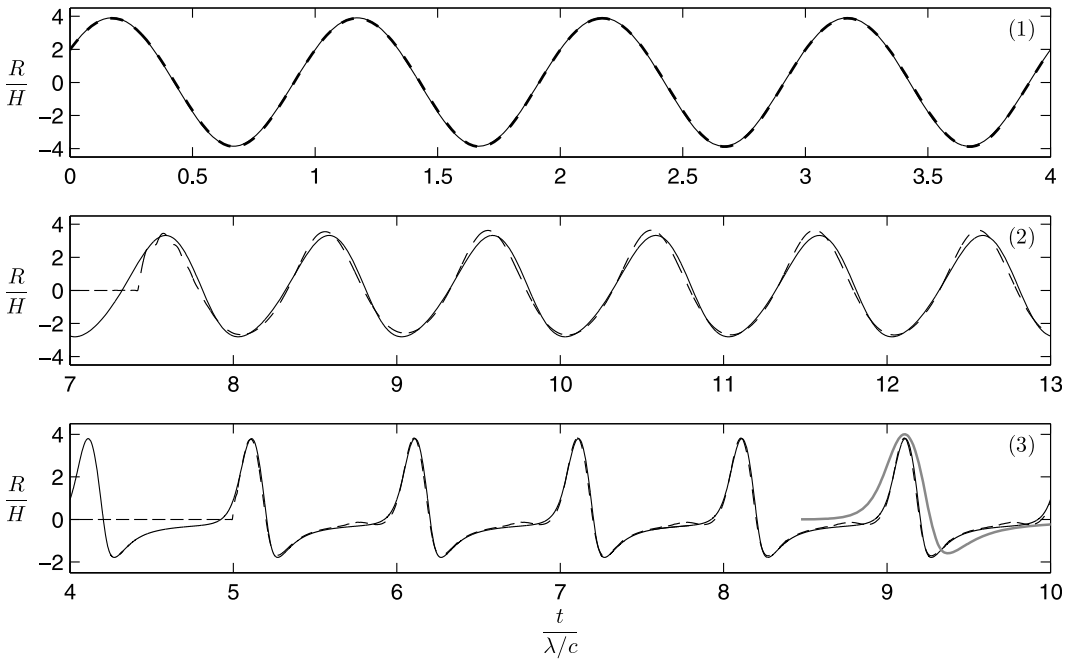

Figure 7. Runup of cnoidal waves on a two-slope beach with $s = 1/20$. Case 1: $m = 0.05$, $\epsilon = 0.001$; case 2: $m = 0.5$, $\epsilon = 0.005$; case 3: $m = 0.9995$, $\epsilon = 0.01$. Solid lines show the analytical solutions, (19). Dashed line in case 1 plots the analytical solution of the comparable (i.e., same ϵ as the cnoidal waves) linear progressive wave. In cases 2 and 3 dashed lines are the corresponding numerical results. The thick line in case 3 plots the solution of a comparable solitary wave.

[25] The present analytical solutions are also compared with the existing laboratory studies. Figures 8 and 9 show comparisons of the analytical solutions with experimental data reported by *Ohyama* [1987] and *Synolakis et al.* [1988], respectively. Figure 8 plots the runup results on a two-slope beach with $s = 1$ (i.e., 45°) for various wave amplitudes ($0 < \epsilon < 0.3$) and wave periods $\left(T/\sqrt{h_0/g} = 12, 14, 16\right)$. In all cases, the constant depth is fixed at $h_0 = 0.2$ m.Analytical solutions agree reasonably well with the measurements, as shown in Figure 8. The discrepancy, however, becomes considerable for larger waves. In the same figure, we also plot the linear solution by *Synolakis et al.* [1988], i.e., (17). Our solutions agree well with their results, although the difference can still be seen. For the case discussed in Figure 9, the slope is again $s = 1$. While the wave nonlinearity is now fixed at $\epsilon = 0.1$, the dimensionless wavelength varies in the range of $10 \lesssim L/h_0 \lesssim 70$. We remark that by definition $L/h_0 = T/\sqrt{h_0/g}$. In addition to the laboratory measurements and the present analytical solutions, in Figure 9 we also plot our Lagrangian numerical results, the numerical simulations by *Liu and Cho* [1994], who solved the fully nonlinear potential flow using the boundary integral equation method, and the original analytical solutions by *Synolakis et al.* [1988] [see *Synolakis et al.*, 1988, Figure 2]. As a reference, the numerical runup solution for a solitary wave, which is the limiting case of cnoidal waves as $m \to 1$,

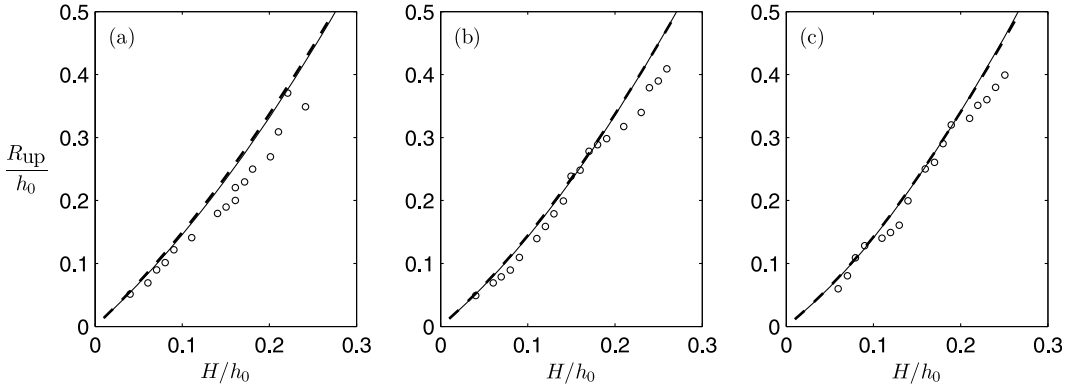

Figure 8. Comparison of maximum runup height, R_{up}, of cnoidal waves on a 45° slope. The constant water depth is $h_0 = 0.2$ m The dimensionless wave periods, $T/\sqrt{h_0/g}$, are: (a) 12, (b) 14, and (c) 16. Symbols are the experimental data of *Ohyama* [1987]. Solid lines plot the present analytical solutions, (19), and the dashed lines show the modified solutions of *Synolakis et al.* [1988], i.e., (17).

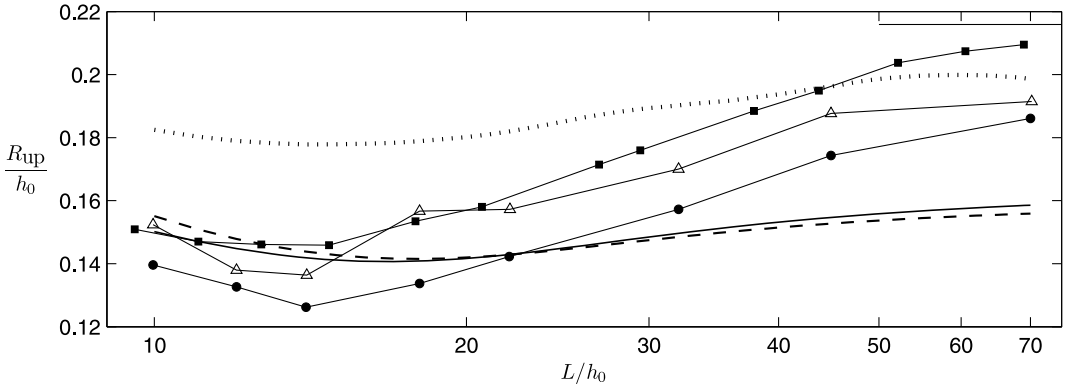

Figure 9. Maximum runup height ($R_{\rm up}$) of cnoidal waves running up 1 : 1 slope. The wave nonlinearity is fixed at $\epsilon = 0.1$. Connected circles are the experimental data of *Synolakis et al.* [1988]. The solid line plots the present analytical solution, (19). The dotted line shows the original analytical solution given by *Synolakis et al.* [1988] (see Figure 2 in their paper) and the dashed line is their solution with our modifications as given in (17), respectively. Connected squares: Lagrangian numerical results. Connected triangles: numerical (BIEM) simulations by *Liu and Cho* [1994]. The horizontal bar denotes the runup height of a amplitude-comparable solitary wave obtained by *Liu and Cho* [1994].

is also indicated. We note that for $L/h_0 = 70$, $m \approx 0.9999999$. All results shown in Figure 9 demonstrate a qualitative agreement that with a fixed ϵ value the runup height of cnoidal waves grows with the increasing wavelength for $L/h_0 > 20$. As the wavelength increases, the Ursell number ($U_r = \epsilon L^2/h_0^2$) and the skewness of cnoidal waves also increase. This leads to higher wave crests for the same wave height (i.e., same ϵ value), and correspondingly it results in higher runup height. Figure 9 has also shown that two numerical results (BIEM and Lagrangian) agree reasonably with each other. Our Lagrangian prediction, which approaches the solitary wave asymptote at larger value of L/h_0, is higher than that of *Liu and Cho* [1994] as the bottom friction has been considered in their simulations. Regrading the analytical solutions, our new result agrees well with that modified from *Synolakis et al.* [1988], i.e., (17), but is very different from their original solution [see *Synolakis et al.*, 1988, Figure 2]. The maximum difference between the analytical solutions and the numerical results is around 12%. This discrepancy is mainly due to the use of the asymptotic forms for the Bessel functions in deriving the analytical solutions, which has been discussed in detail by *Liu and Cho* [1994].

3.2. Runup of Multiple Solitary Waves

[26] *Madsen et al.* [2008] have advocated that solitary wave is not a good model wave for leading tsunamis. Instead, the leading waves from a surface disturbance is an undular bore. In several of their numerical examples, it is interesting to see that these bores are often consist of a series of overlapping soliton-like waves (more rigorously, the trailing wave can be fitted by a train of modulated cnoidal waves as has been suggested by the earlier studies [e.g., *Peregrine*, 1966; *Gurevich and Pitaevskii*, 1974]). The runup of undular bores can surely be simulated numerically using our Lagrangian model, or estimated by the integral formula, (9). However, to understand how the trailing waves and the first few waves affect each other during the runup process we study the runup of a group of solitary waves. Towards this goal, we can again take advantage of the existing analytical solution for a single solitary wave. In a constant depth region, interaction of solitary waves has been studied [see, e.g., *Whitham*, 1974]. One of the main results is the elastic interaction of solitary waves: these waves preserve their identities (at least to the leading-order solution). Thus, for our runup study we shall consider an episode where the record of incident waves at the beach toe is the linear superposition of two solitary waves:

$$\Phi(t) = H\mathrm{sech}^2[\Omega(t-t_1)] + (\alpha H)\mathrm{sech}^2[(\beta\Omega)(t-t_2)], \qquad (23)$$

where t_1 and t_2 are phase shifts ($t_2 - t_1$ represents the time separation between two wave crests) and α and β denote the amplitude and frequency ratios, respectively. For two solitary waves, $\Omega \approx h_0^{-1}\sqrt{3H/4h_0}\sqrt{gh_0}$ and consequently $\beta = \sqrt{\alpha}$. In section 3.3 we will revisit this problem when α and β do not satisfy this condition, which is the case of the leading tsunami waves at Iwate South. To provide a quantitative picture of the combined waves with various α and $t_2 - t_1$, in Figure 10 we show the time histories of incident waves at the beach toe, representing two successive solitary waves with five values of amplitude ratio along with three separation intervals. If two waves are very close, the wave crests become indistinguishable, which is less interesting. On the other hand, if two solitary waves are far apart, they are independent of each other and the runup solutions are the same as those for each individual wave.

[27] The shoreline solutions, $R(\tau)$ and $U(\tau)$, for the incoming wave form given in (23) can be readily deduced from (13). In many cases, we are more interested in the maximum runup and drawdown. Therefore, it is useful to define

$$\begin{cases} R_{\rm up} = \max\left\{\dfrac{R(\tau)}{h_0}\right\} = \mathcal{M}_{\rm up}\ s^{-\frac{1}{2}}\left(\dfrac{H}{h_0}\right)^{\frac{5}{4}}, \\ R_{\rm down} = \min\left\{\dfrac{R(\tau)}{h_0}\right\} = \mathcal{M}_{\rm down}\ s^{-\frac{1}{2}}\left(\dfrac{H}{h_0}\right)^{\frac{5}{4}}. \end{cases} \qquad (24)$$

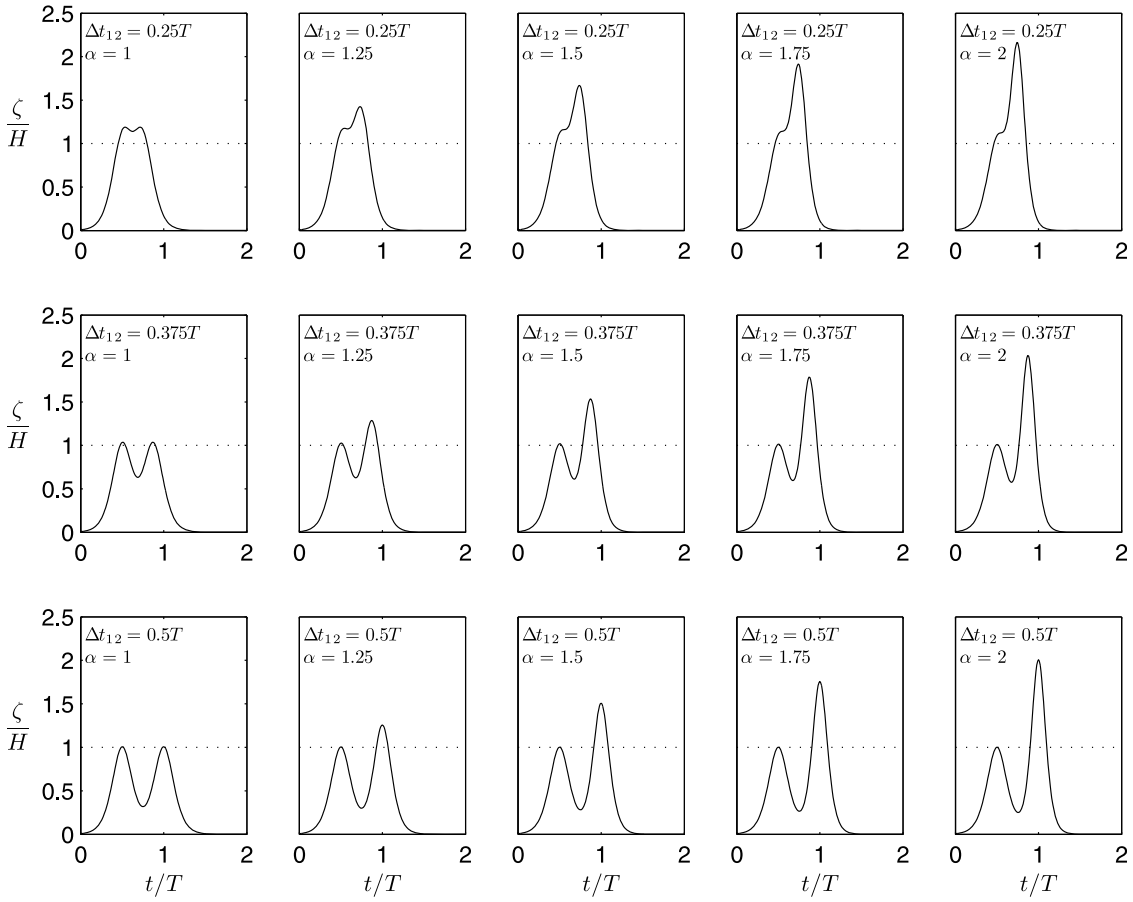

Figure 10. Two successive solitary waves with different amplitude ratio, α, and separation time, $\Delta t_{12} = t_2 - t_1$: records of incident waves at the beach toe, $x = X_0$. Here $T = 2\pi\Omega^{-1}$ is the effective wave period of the first wave.

Clearly, both $\mathcal{M}_{\text{up}}$ and $\mathcal{M}_{\text{down}}$ are functions of amplitude ratio, α, and the separation time of the two successive solitary waves, $t_2 - t_1$. From (14), the associated theoretical breaking condition is also obtained as

$$\frac{H}{h_0} \le \left[\left(\frac{3}{4}\right)^{-\frac{5}{4}} \frac{1}{32\sqrt{2\pi}} \frac{-1}{\Theta_{\text{B}}\left(-\frac{7}{2}, \theta_{\text{breaking}}\right)}\right]^{\frac{9}{4}} s^{\frac{10}{9}}, \tag{25}$$

where

$$\Theta_{\text{B}}(m,\theta) = \text{Li}\left(m, -e^{2\theta}\right) + \beta^{\frac{3}{2}}\text{Li}\left(m, -e^{2\beta(\theta+\Omega(t_1-t_2))}\right),$$

and $\theta = \theta_{\text{breaking}}$ is the roots of

$$\text{Li}\left(-\frac{9}{2}, -e^{2\theta}\right) + \alpha\beta^{-\frac{1}{2}}\text{Li}\left(-\frac{9}{2}, -e^{2\beta(\theta+\Omega(t_1-t_2))}\right) = 0.$$

Similar to (24), we can rewrite the breaking condition in the following form:

$$\varepsilon_{\text{breaking}} = \frac{H}{h_0}\bigg|_{\text{breaking}} = \mathcal{B}\ s^{\frac{10}{9}} \tag{26}$$

In Figure 11, we present the runup factors as function of α varying from 1 to 2.5, with $(t_2 - t_1)/T = 0.25, 0.375, 0.5$. The corresponding wave breaking condition is also given in Figure 12. We observe that for both runup and drawdown events the breaking conditions of the combined wave are more restricted than those of each individual solitary wave (i.e., in Figure 12 values of $\mathcal{B}$ denoted by symbols (for the combined waves) are smaller than those depicted by dotted lines (for single solitary wave)). The results also reveal that the factor $\mathcal{M}_{\text{up}}$ of the combined waves is smaller (i.e., symbols are below the dotted line as shown in the plot), which implies a lower maximum runup height. This can be explained as follows. The runup associated with the second wave is weaken by the drawdown of the first wave. However, the opposite is shown for the drawdown: the magnitude of $\mathcal{M}_{\text{down}}$ is larger for the combined waves. The stronger overall drawdown can be seen as the rundown flow of the first wave being carried up by the second runup, but eventually this combined upward flow must descend towards the toe. We reiterate that all the discussions presented here are for non-breaking waves. The behavior is expected to be more complicated if waves break on the sloping beach.

[28] In a separate calculation (not presented here), we also study the runup behavior of two iso-scale solitary waves (i.e., $\alpha = 1$) as a functions of $t_2 - t_1$. We observe similar results: the maximum runup height is achieved by the first wave, but it becomes the same as that for the single wave for

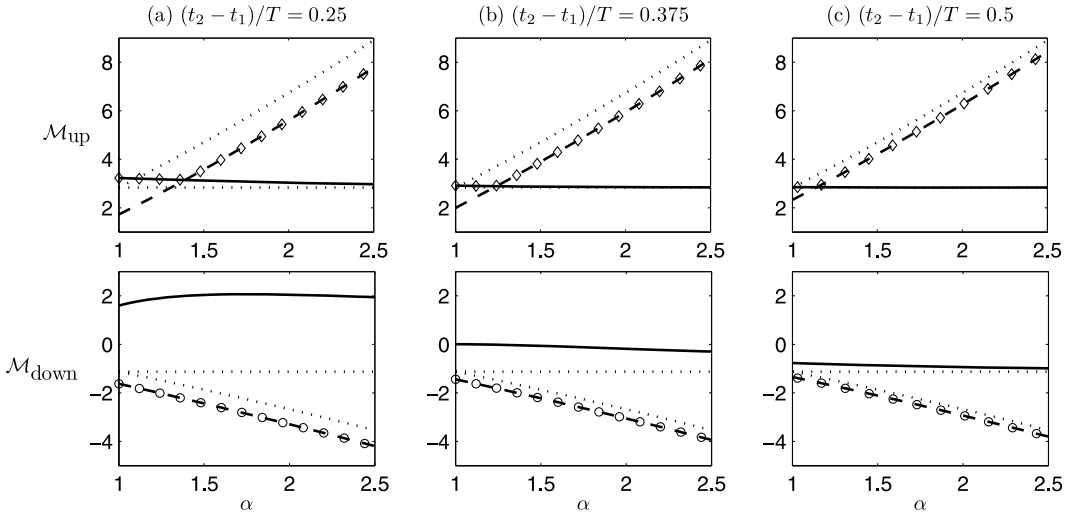

Figure 11. Runup factors for two successive solitary waves as functions of α under three different values of $t_2 - t_1$. (top) The factors for the runup extremes $\mathcal{M}_{\rm up}$. (bottom) The maximum drawdown, $\mathcal{M}_{\rm down}$. The overall solutions for the combined incident waves are denoted by the symbols. Solid and dashed lines represent the results of the first and the second runup/drawdown, respectively. Finally, dotted lines plot the reference solutions of each individual wave.

$(t_2 - t_1)/T \gtrsim 0.5$; the second runup is always weaken by the drawdown of the first wave; the overall rundown flow of the combined wave is always stronger than that of a single wave, but the difference becomes negligible for large wave separation time.

[29] Finally, in Figure 13 we discuss the detailed shoreline evolution by considering a specific case of two iso-scale solitary waves running up a 1 : 20 slope. The wave nonlinearity is $\epsilon = 0.01$ and the initial separation time between two waves is $0.5T$. Figure 13a plots the initial surface profile. Records of surface elevation at select locations are also illustrated in Figures 13b and 13c. Comparing to the runup of a single solitary wave shown in Figure 4, we can see that the second peaks in Figures 13b and 13c are much larger than those of the single wave case. This is due to the drawdown of the first wave meets with the runup of the second wave. However, the runup solution shown in Figure 13e reveals that the runup of the first wave is not affected by the following wave and yields the maximum runup height. We also check our analytical solutions with the direct numerical calculations. A good agreement between two solutions is observed, as shown in Figure 13.

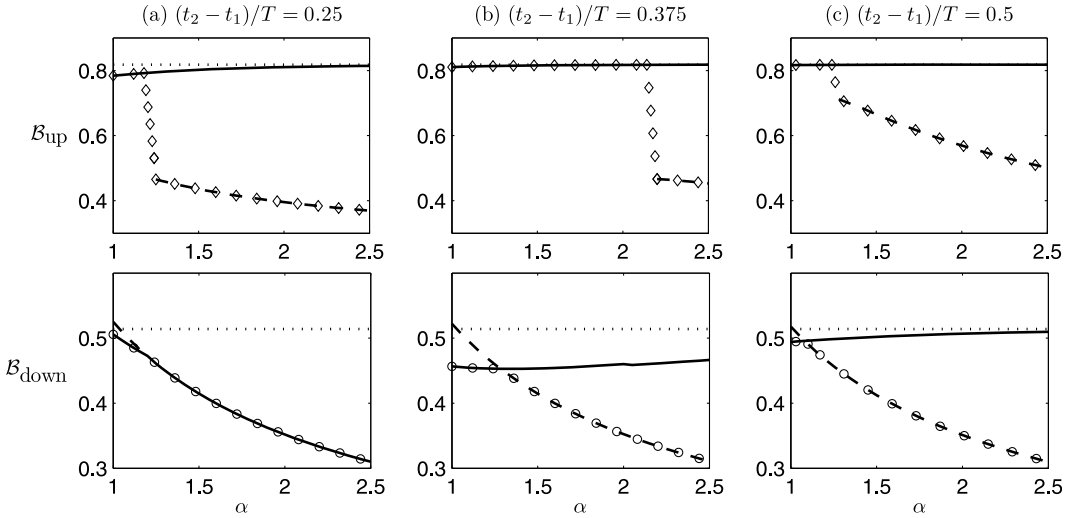

Figure 12. Wave breaking conditions for two successive solitary waves as functions of α under three different values of $t_2 - t_1$. (top) The factors for the runup process $\mathcal{B}_{\rm up}$. (bottom) The drawdown event, $\mathcal{B}_{\rm down}$. Symbols denotes the overall results for the combined incident waves. Solid and dashed lines are the corresponding results of the first and the second runup/drawdown. Dotted lines plot the reference solutions of each individual wave.

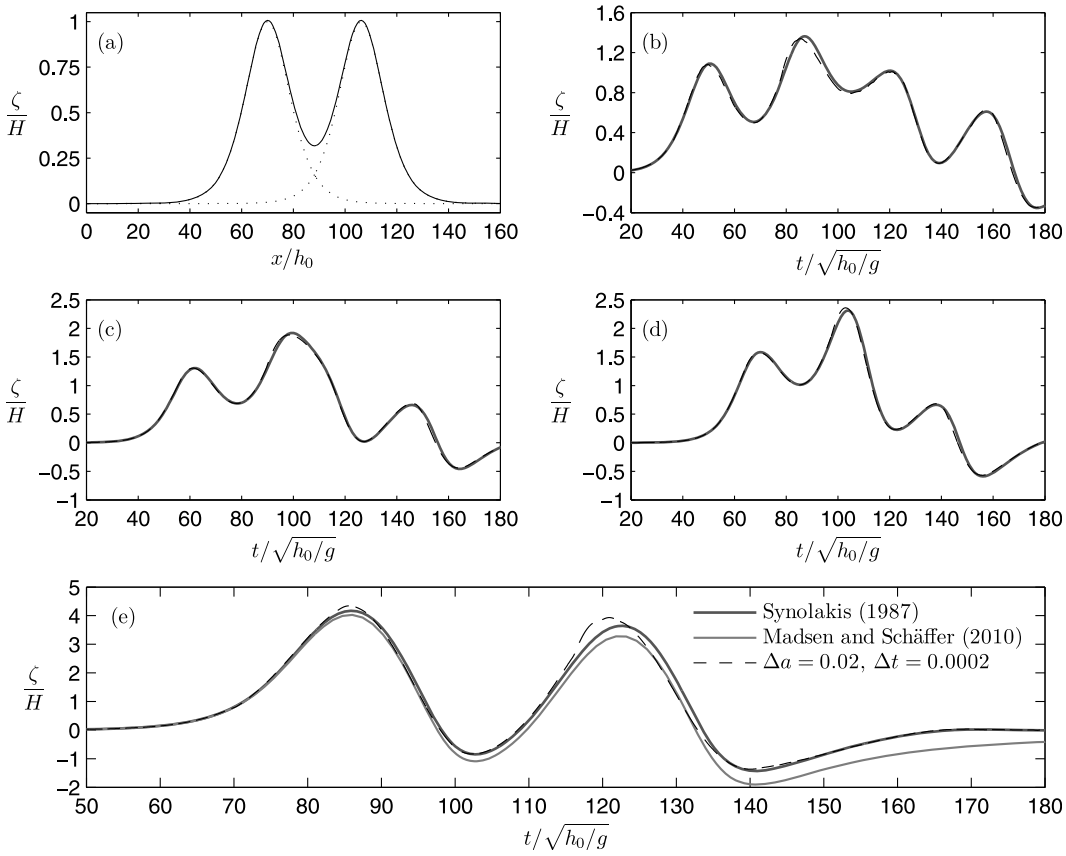

Figure 13. Runup of two iso-scale solitary waves on a 1-on-20 slope. (a) Initial condition. The separation time between two solitary waves is $0.5T$. The wave nonlinearity is $\epsilon = 0.01$. The dashed line plots the reference solitary waves. (b) Records of surface elevation at the beach toe, $x = X_0$. The solid line plots the analytical solution and the dashed line is the numerical results. (c and d) Records at $x/X_0 = 0.1$, 0.05, respectively. (e) Evolution of the shoreline.

3.3. Estimation of Runup Height at Iwate South

[30] We now discuss the runup of leading tsunamis using the gauge record at the Iwate South GPS station (see Figure 2) as an example. For simplicity, we adopt a two-slope beach by assuming a constant depth region in the offshore direction from the Iwate South station. Using the linear long-wave speed, we translate the surface elevation record at Iwate South along with two proposed approximations shown in Figure 2, i.e., a single $\mathrm{sech}^2(\cdot)$ wave and a combination of three soliton-like profiles, into the initial wave profiles. These incident wave forms are plotted in Figure 14a. We reiterate that the runup solutions for a $\mathrm{sech}^2(\cdot)$ wave and the wave packet described by (3) are already known from (13). In Figure 14b, we compare the analytical runup solutions of these two approximate wave profiles with the calculation using the gauge measurements. All three solutions suggest a similar maximum runup height approximately of 12.5 m. In addition, the combined wave packet actually describes the entire runup process quite well. For the drawdown event, both approximate incident waves are unable to describe the oscillations, as can be expected. We note that in this demonstration a beach slope of $s = 1/10$ has been assumed. However, a crude constant slope from the GPS station to the shore is $s = \frac{204\ \mathrm{m}}{14\ \mathrm{km}} \approx 1 : 70$. On the one hand, the chosen of a steeper slope is to avoid unwanted wave breaking, which is not considered in this study. On the other hand, the bathymetry at the real shoreline, which has a dominant effect on the runup as suggested by *Kânoğlu and Synolakis* [1998], must have a much steeper slope, i.e., $s \gg 1/70$. Of course, we have no intention to argue that the $1 : 10$ slope is representative to the real bathymetry. For the record, the surveyed runup height in this region (Kamaishi bay area) is around 17 m [*Takahashi et al.*, 2011]. This example again suggests that a good description of the front profile of the leading tsunamis is sufficient to give a reasonable estimation of the maximum runup height. Analytical solutions are also possible by the use of fundamental solutions given by *Madsen and Schäffer* [2010] provided a two-slope beach is assumed.

4. Key Factors Affecting the Maximum Runup Height

[31] We have demonstrated in the previous sections that solitary waves may not be adequate representations of leading tsunamis since for a specified wave height the characteristic wave period of a solitary wave is usually too short with respect to the leading tsunami wave. We have also extended the analytical approach to study the runup of a train of multiple waves. Here we shall further examine specifically the effect of the scale factor on the runup process and

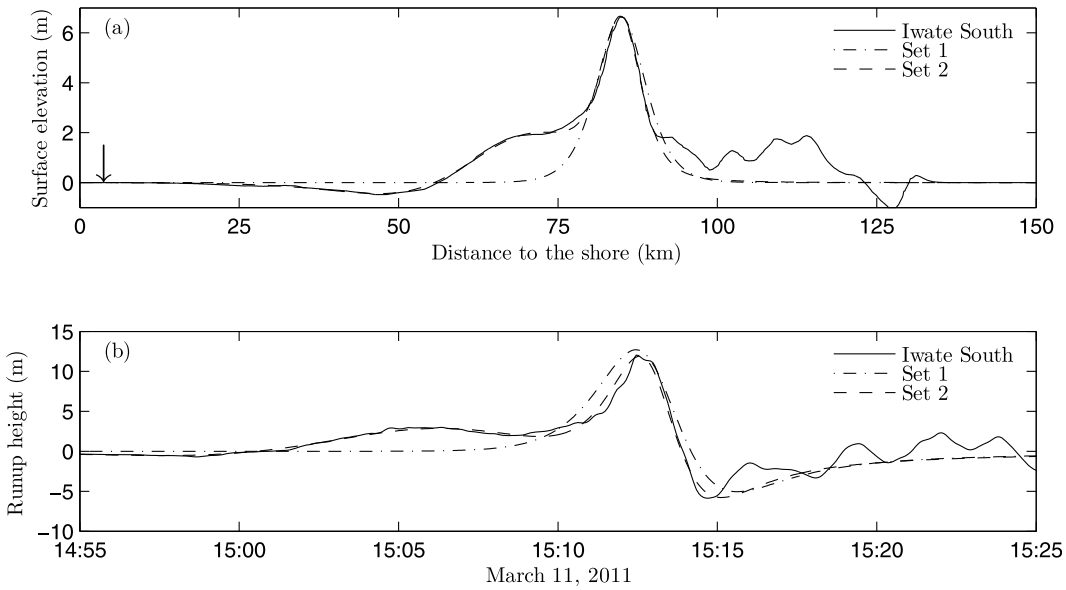

Figure 14. Runup of leading tsunami waves. (a) Initial wave profiles. Iwate South: record from the GPS station. Set 1: a single sech$^2(\cdot)$-profile approximation. Set 2: a wave packet consisting of three soliton-like profiles, see (3). The arrow indicates the location of the beach toe. (b) Shoreline locations. A two-slope beach assumed with $s = 1/10$ and $h_0 = 204$ m.

then demonstrate that the analytical approach can, in principle, be applied to estimate the maximum runup height of leading tsunami waves.

[32] Figure 15 discusses three different sech$^2(\cdot)$-shape incident waves, indicated in (1), with a same wave height H but different wavenumbers k (or effective wavelengths $L = 2\pi/k$). The reference is a solitary wave with $k = k_0$ defined by (2). As can be expected, the numerical results show that the widest incident waves reaches the shoreline sooner than the other two events. However, the narrowest incident wave yields the largest maximum runup and drawdown elevations even though it carries the least amount of water mass. This can be explained from the momentum equation, (5), which suggests that the acceleration of the water particles is driven by the pressure gradient force (or equivalently the magnitude of ζ_x). As the frequency dispersion is neglected in our analysis, we can further assume that for an incident wave of single wave form the accelerating phase ($\partial\, \zeta_{inc}/\partial x > 0$) is responsible for the runup process and the maximum runup elevation while the deceleration phase

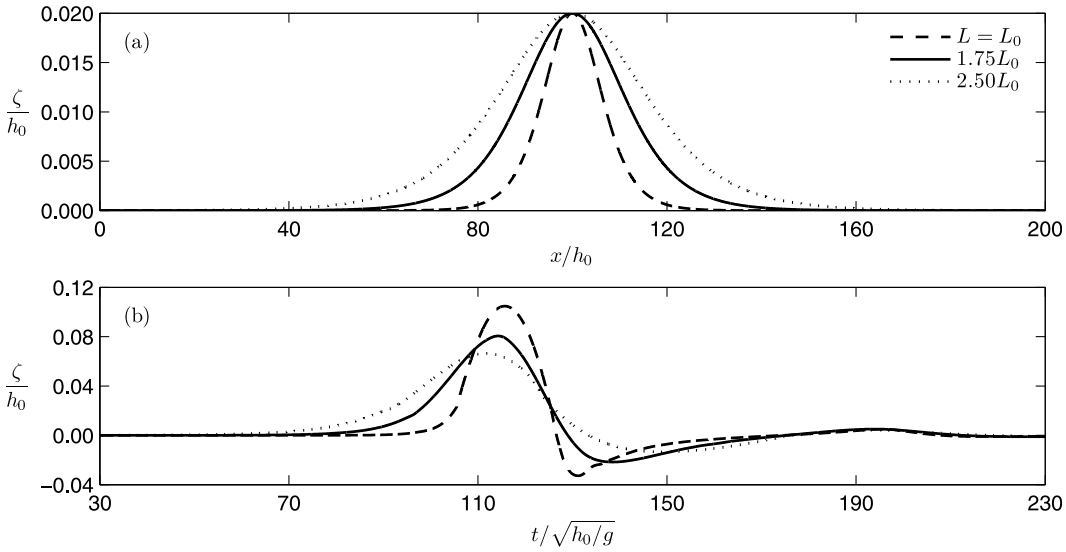

Figure 15. Runup of three different sech$^2(\cdot)$-shape waves with the same wave height but different wavelengths. (a) Incident wave forms. (b) Evolutions of the shoreline tips. The reference wavelength, $L_0 = 2\pi/k_0$, is the effective wavelength of a solitary wave as defined in (1) and (2). Locations of the wave crests are chosen such that the waves are all initiated in the constant depth region. In this example, the beach slope is $s = 1/20$.

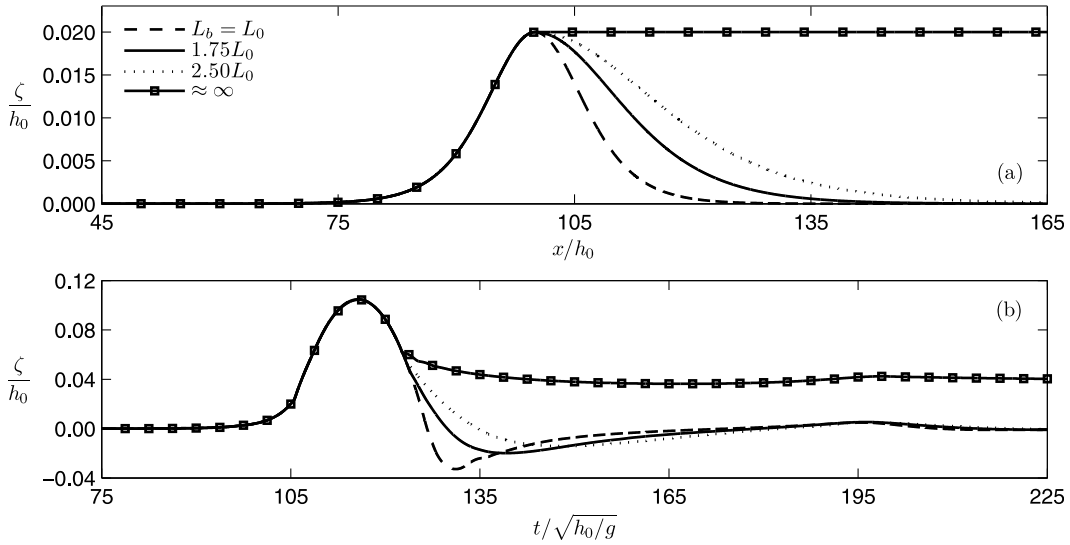

Figure 16. Effects of back-profiles of the initial waves on the runup and drawdown. (a) Incident wave forms. (b) Evolutions of the shoreline. All incidents waves have the same front shape as a solitary wave ($L = L_0$). The reference back-profile is also a solitary wave, i.e., $L_b = L_0$. The case $L_b = \infty$ illustrates a uniform bore. The beach slope is $s = 1/20$.

($\partial\zeta_{inc}/\partial x < 0$) plays a more important role during the drawdown event. In fact, this can also be inferred from the analytical solution, (9), which states that the shoreline position, $R(\tau)$, is the convolution integral of Φ_t (Φ_t is equivalent to ζ_x, see (8)). To illustrate this idea further, we test several asymmetric incident waves that have identical wave front (i.e., acceleration phase) but different back-profiles (i.e., deceleration phase). To be more precise, these waves can all be described by $\mathrm{sech}^2(\cdot)$-profiles but employing different wavenumbers for the accelerating phases and the back-profiles. The incident wave forms are depicted in Figure 16a. Clearly, this example suggests that back-profiles play no role in the runup process and the maximum runup elevation remains the same, as shown in Figure 16b. The deceleration history, instead, determines the drawdown process. In addition, the wider back-profiles (i.e., weaker $|\zeta_x|$) yield smaller maximum drawdown elevations. This is consistent with those shown in Figure 15. We also examine an extreme case of infinitesimal wavenumber for the backprofile ($L_b = \infty$ in Figure 15), which illustrates a uniform bore. The solution shows that the water level eventually settles at the level that is twice the initial wave height as the results of superposition of two opposing bores. The fact that an equilibrium state is reached at the shoreline can also be seen from the analytical, (9), since $\Phi_t = 0$ at large time. We remark that the behaviors demonstrated in Figures 15 and 16 are also applied to leading depression waves, although the results are not presented here.

[33] Through the above examples, we confirm that the time scale of an incident wave indeed has a significant effect on the runup. Our results also suggest that knowing the front-profile of the incoming wave alone is sufficient to estimate the runup of a single wave. These findings are significant as in tsunami hazard forecasting and warning practices the maximum runup height is one of the most important information. One the one hand, we realize that the runup estimations based on the solitary wave theory are often conservative, as in shallow waters amplitude-comparable solitary waves have much smaller wavelengths than those of leading tsunamis (see the example of 2011 Tohoku event shown in Figure 2). On the other hand, the analytical approach can provide a quick and reasonable assessment on the runup of leading tsunamis if the front-profile of the incident wave is known. This has been demonstrated in section 3.3 by considering the wave record at Iwate South. We reiterate that the above statements are based on the assumption that waves do not break. In this section we consider only single waves, whereas the real leading tsunami waves can often be viewed as wave packets consisting of several waves. It is anticipated that a prominent peak exists in the leading wave packet, as was the case at TM1, TM2, and Iwate South stations shown in Figure 1. Whether this hypothesis is generally true for tsunami waves relies on further detailed study of the leading waves, either by simplified theoretical arguments or empirical examination on more field observations. In nearshore regions, the evolution of leading tsunamis depends strongly on the bathymetry. However, in deep ocean the waveform of leading waves can be roughly estimated by the theory of *Kajiura* [1963], which describes waves evolving from surface disturbances or ground motions in a constant depth. Although the theoretical estimation on the waveform and eventually the analytical runup height are not as accurate as the sophisticated numerical simulations, they can still provide swift qualitative information on the leading tsunami waves.

5. Concluding Remarks

[34] In this note, we studied the evolution of non-breaking long waves on a simple two-slope beach. Using the numerical model based on the Lagrangian long-wave equations, we have identified that for a single wave the runup process is controlled by the accelerating phase while the drawdown flow is mainly dominated by the back-profile. This suggests

that as far as the maximum runup height is concerned, one should focus on better describing the front profile of the leading tsunami waves. We also extended the analytical approach of *Madsen and Schäffer* [2010] to study the runup formulae of cnoidal waves and a train of several solitary waves. It is shown that the shoreline solutions for a solitary wave, or a sinusoidal wave, can be used to obtain the solutions for these more complex waves. The analytical wave-breaking condition can also be deduced. For the runup of two solitary waves where a wave is followed by one with a larger amplitude, we found that the maximum runup is slightly smaller than that of a single solitary wave. However, the overall drawdown flow becomes much stronger. Consequently, the wave breaking is more restrictive. To connect to the study of tsunamis, we used the analytical approach to estimate the runup of leading waves recorded from the 2011 Japan Tohoku tsunami. It is demonstrated that using a single $\mathrm{sech}^2(\cdot)$ or the combination of several $\mathrm{sech}^2(\cdot)$ profiles, the maximum runup height can be approximated reasonably. The present study is partially motivated by *Madsen et al.* [2008] who advocated to clarify the solitary wave paradigm on tsunamis. By examining the field data taken during the 2011 Tohoku tsunami, indeed we supported that solitary waves are not ideal model waves for tsunamis. However, we have considered only one horizontal dimension. It is known that the evolution of an initial surface hump on a two-dimensional plane can behave differently [see, e.g., *Kajiura*, 1963], the range of validity of solitary wave theory in two-dimensional spreading deserves a separate examination.

[35] **Acknowledgments.** The research work presented here is supported by grants from the National Science Foundation and the Office of Naval Research to Cornell University.

References

Boyd, J. P. (1984), Cnoidal waves as exact sums of repeated solitary waves: New series for elliptic functions, *SIAM J. Appl. Math.*, *44*, 952–955.

Carrier, G., and H. P. Greenspan (1958), Water waves of finite amplitude on a sloping beach, *J. Fluid Mech.*, *4*, 97–109.

Carrier, G., T. T. Wu, and H. Yeh (2003), Tsunami runup and draw-down on a plane beach, *J. Fluid Mech.*, *475*, 79–99.

Fujii, Y., K. Satake, S. Sakai, M. Shinohara, and T. Kanazawa (2011), Tsunami source of the 2011 off the Pacific coast of Tohoku earthquake, *Earth Planets Space*, *63*, 815–820.

Fujima, K. (2007), Tsunami runup in Lagrangian description, in *Tsunami and Nonlinear Waves*, edited by A. Kundu, pp. 191–208, Springer, New York.

Gjevik, B., and G. Pedersen (1981), Run-up of long waves on an inclined plane, report, Dep. of Math., University of Oslo, Oslo.

Goring, D., and F. Raichlen (1980), The generation of long waves in the laboratory, paper presented at 17th International Conference on Coastal Engineering, Am. Soc. of Civ. Eng., Sydney, N. S. W., Australia.

Goto, C. (1979), Nonlinear equation of long waves in the Lagrangian description, *Coastal Eng. Jpn.*, *22*, 1–9.

Gurevich, A. V., and L. P. Pitaevskii (1974), Nonstationary structure of a collisionless shock wave, *Sov. Phys. JETP*, *38*, 291–297.

Hammack, J. L., and H. Segur (1978), Modelling criteria for long water waves, *J. Fluid Mech.*, *84*, 359–373.

Kajiura, K. (1963), The leading wave of a tsunami, *Bull. Earthquake Res.*, *41*, 525–571.

Kânoğlu, U. (2004), Nonlinear evolution and runup–rundown of long waves over a sloping beach, *J. Fluid Mech.*, *513*, 363–372.

Kânoğlu, U., and C. E. Synolakis (1998), Long wave runup on piecewise linear topographies, *J. Fluid Mech.*, *374*, 1–28.

Keller, J. B., and H. B. Keller (1964), Water wave run-up on a beach, *PNR Research Rep. NR-3828(00)*, Dep. of the Navy, Washington, D. C.

Li, Y., and F. Raichlen (2001), Solitary wave runup on plane slopes, *J. Waterw. Port Coastal Ocean Eng.*, *127*, 33–44.

Liu, P. L.-F., and Y.-S. Cho (1994), Integral equation model for wave propagation with bottom frictions, *J. Waterw. Port Coastal Ocean Eng.*, *120*, 594–608.

Madsen, P. A. and H. A. Schäffer (2010), Analytical solutions for tsunami runup on a plane beach: Single waves, *N*-waves and transient waves, *J. Fluid Mech.*, *645*, 27–57.

Madsen, P. A., D. R. Fuhrman, and H. A. Schäffer (2008), On the solitary wave paradigm for tsunamis, *J. Geophys. Res.*, *113*, C12012, doi:10.1029/2008JC004932.

Mei, C. C., M. Stiassnie, and D. K.-P. Yue (2005), *Theory and Applications of Ocean Surface Waves*, World Sci., Singapore.

Ohyama, T. (1987), A boundary element analysis for cnoidal wave runup, *Proc. Jpn. Soc. Civ. Eng.*, *381*, 189–198.

Peregrine, D. H. (1966), Calculations of the development of an undular bore, *J. Fluid Mech.*, *25*, 321–330.

Segur, H. (2007), Waves in shallow water, with emphasis on the tsunami of 2004, in *Tsunami and Nonlinear Waves*, edited by A. Kundu, pp. 3–29, Springer, New York.

Synolakis, C. E. (1987), The runup of solitary waves, *J. Fluid Mech.*, *185*, 523–545.

Synolakis, C. E., M. K. Deb, and J. E. Skjelbreia (1988), The anomalous behavior of the run-up of cnoidal waves, *Phys. Fluids*, *31*, 3–5.

Synolakis, C. E., E. N. Bernard, V. V. Titov, U. Kânoğlu, and F. González (2008), Validation and verification of tsunami numerical models, *Pure Appl. Geophys.*, *165*, 2197–2228.

Takahashi, S., Y. Kuriyama, T. Tomita, Y. Kawai, T. Arikawa, D. Tasumi, and T. Negi (2011), Urgent survey for 2011 Great East Japan Earthquake and Tsunami disaster in ports and coasts, *Tech. Note Port Airport Res. Inst. 31*, Port and Airport Res. Inst., Yokosuka, Japan.

Wang, X., and P. L.-F. Liu (2007), Numerical simulations of the 2004 Indian Ocean Tsunamis—Coastal effects, *J. Earthquakes Tsunami*, *1*, 273–297.

Whitham, G. B. (1974), *Linear and Nonlinear Waves*, Wiley-Interscience, New York.

Whittaker, E. T., and G. N. Watson (1927), *A Course of Modern Analysis*. Cambridge Univ. Press, Cambridge, N. Y.